

Research Paper

SYTL4 downregulates microtubule stability and confers paclitaxel resistance in triple-negative breast cancer

Xi-Yu Liu^{1#}, Wang Jiang^{2#}, Ding Ma¹, Li-Ping Ge¹, Yun-Song Yang¹, Zong-Chao Gou¹, Xiao-En Xu¹, Zhi-Ming Shao¹✉ and Yi-Zhou Jiang¹✉

1. Key Laboratory of Breast Cancer in Shanghai, Department of Breast Surgery, Fudan University Shanghai Cancer Center; Department of Oncology, Shanghai Medical College, Fudan University, Shanghai 200032, China.
2. University of Chinese Academy of Sciences, Beijing 100049, China.

#These authors contributed equally to this work.

✉ Corresponding authors: Dr. Yi-Zhou Jiang, Fudan University Shanghai Cancer Center, No. 270 Dong'an Road, Shanghai, 200032, P.R. China, E-mail: yizhoujiang@fudan.edu.cn; Dr. Zhi-Ming Shao, Fudan University Shanghai Cancer Center, No. 270 Dong'an Road, Shanghai, 200032, P.R. China, E-mail: zhimingshao@yahoo.com.

© The author(s). This is an open access article distributed under the terms of the Creative Commons Attribution License (<https://creativecommons.org/licenses/by/4.0/>). See <http://ivyspring.com/terms> for full terms and conditions.

Received: 2020.02.22; Accepted: 2020.08.09; Published: 2020.08.29

Abstract

Background: Taxanes are frontline chemotherapeutic drugs for patients with triple-negative breast cancer (TNBC); however, chemoresistance reduces their effectiveness. We hypothesized that the molecular profiling of tumor samples before and after neoadjuvant chemotherapy (NAC) would help identify genes associated with drug resistance.

Methods: We sequenced 10 samples by RNA-seq from 8 NAC patients with TNBC: 3 patients with a pathologic complete response (pCR) and the other 5 with non-pCR. Differentially expressed genes that predicted chemotherapy response were selected for *in vitro* functional screening via a small-scale siRNAs pool. The clinical and functional significance of the gene of interest in TNBC was further investigated *in vitro* and *in vivo*, and biochemical assays and imaging analysis were applied to study the mechanisms.

Results: Synaptotagmin-like 4 (SYTL4), a Rab effector in vesicle transport, was identified as a leading functional candidate. High SYTL4 expression indicated a poor prognosis in multiple TNBC cohorts, specifically in taxane-treated TNBCs. SYTL4 was identified as a novel chemoresistant gene as validated in TNBC cells, a mouse model and patient-derived organoids. Mechanistically, downregulating SYTL4 stabilized the microtubule network and slowed down microtubule growth rate. Furthermore, SYTL4 colocalized with microtubules and interacted with microtubules through its middle region containing the linker and C2A domain. Finally, we found that SYTL4 was able to bind microtubules and inhibit the *in vitro* microtubule polymerization.

Conclusion: SYTL4 is a novel chemoresistant gene in TNBC and its upregulation indicates poor prognosis in taxane-treated TNBC. Further, SYTL4 directly binds microtubules and decreases microtubule stability.

Key words: Triple-negative breast cancer, paclitaxel resistance, SYTL4, microtubule polymerization

Introduction

Breast cancer is the most common cancer that threatens the health of women worldwide [1]. Triple-negative breast cancer (TNBC), defined by the lack of expression of the estrogen receptor (ER), the progesterone receptor (PR) and the human epidermal growth factor receptor (HER2) [2], comprises 12-20% of breast cancers and is characterized by poor prognosis, early metastasis, and aggressive tumor behavior [3, 4]. Our recent study classified TNBC into

four different subtypes based on transcriptome profiles, namely, luminal androgen receptor (LAR), immunomodulatory (IM), basal-like immune-suppressed (BLIS), and mesenchymal (MES), suggesting that TNBC itself is heterogeneous. Among these subtypes, the MES subtype exhibits the poorest prognosis but lacks distinctive genomic alterations [5, 6]. New potential therapeutic targets are emerging for TNBCs, such as folate receptor alpha (FR α) [7], and

the supernumerary centrosomes [8].

Neoadjuvant chemotherapy (NAC) based on paclitaxel has served as a standard treatment for many patients with TNBC, especially for locally advanced disease [9]. Although a proportion of patients with TNBC show an excellent pathologic complete response (pCR), 30-50% develop resistance, leading to a poor prognosis [10]. Discovering novel oncogenes driving TNBC progression is required for developing new therapeutic targets for TNBC. Several studies have compared transcriptomic differences in pre-NAC samples between responders and nonresponders and established predictive signatures to drug response [11-14]. Furthermore, profiling residual tumors after NAC can identify genes associated with drug resistance via bulk sequencing [15-17] or single-cell sequencing [18]. On the other side, overexpression of drug-efflux pumps [19], alterations in microtubule-associated proteins [20, 21], aberrant cancer stem cell signaling [22, 23], and activated PI3K/Akt pathway [24, 25], etc., have been reported to be associated with chemoresistance.

In this study, we sequenced 10 TNBC tumor samples from 8 patients who received taxane-containing NAC in Fudan University Shanghai Cancer Center (FUSCC). Differentially expressed genes were further screened by *in vitro* siRNA to identify paclitaxel resistance-associated genes.

Materials and Methods

RNA-sequencing and bioinformatic analysis

For tumor RNA-sequencing (RNA-seq), ten freshly frozen tissues were collected from eight patients with TNBC who received neoadjuvant paclitaxel and carboplatin at FUSCC. Among these ten samples, eight were obtained by core needle biopsy as pre-NAC baseline samples, and two were surgically resected tumors as matched post-NAC residual samples from two patients with progressed disease (PD). Core needle biopsies contained 70-90% pure tumor cells with minimal stromal contamination. RNA was isolated using the RNeasy mini kit (Qiagen, Germany) and sequenced by RNA-seq on an Illumina HiSeq 2500 platform by GENESSEQ (Nanjing, China). Reads were aligned to the GRCh37 genome using STAR [26]. Gene expression levels were quantified as transcripts per kilobase million (TPM) using RNA-Seq by Expectation-Maximization (RSEM) [27]. Differentially expressed genes (DEG) were identified using R package 'limma'.

Gene Set Enrichment Analysis and pathway analysis

We analyzed the enriched pathways of

candidate genes in the Kyoto Encyclopedia of Genes and Genomes (KEGG) database (<http://www.genome.jp/kegg/>) [28]. The top 20 enriched KEGG pathways were plotted in a bubble plot. "Rich factor" means the ratio of the number of called genes to the background number annotated in a certain pathway. The greater the "Rich factor", the greater is the degree of enrichment.

We evaluated the differences in expression between the high and low SYTL4-expression groups on a set of 50 hallmark signatures downloaded from MSigDB [29, 30] using the Gene Set Enrichment Analysis (GSEA) software (GSEA 2.2.1, <http://software.broadinstitute.org/gsea/>).

Cell cultures

TNBC cell lines (MDA-MB-231, Hs578T, HCC1143, HCC1937, HCC1599, MDA-MB-157, BT-20, MDA-MB-436, HCC38 and HCC70) and 293T cells were obtained from the American Type Culture Collection (Manassas, VA, USA) and maintained in complete DMEM growth medium containing 10% fetal bovine serum (FBS) (Gibco, USA), 2 mM L-glutamine, 100 IU/mL penicillin, and 100 µg/mL streptomycin [31]. Liquid nitrogen stocks were created upon receipt, and cells were maintained until the start of each study. Cells were used for no more than 10 passages after being thawed. All cell lines tested negative for mycoplasma contamination.

siRNA pool assay

The custom small interfering RNA (siRNA) pool was synthesized with three siRNA duplexes for each gene (RiboBio, China). In total, the pool contains 90 targets for 30 genes and one nontargeting siRNA. To compare the effect of a drug on siRNA-transfected cells with the effect on cells transfected with the nontargeting siRNA, the "sensitization index" (SI) [32] was used: $SI = (Rc/Cc) * (Cd/Cc) - Rd/Cc$, where the symbols represent the absorbance measured after incubating cells with CCK-8 reagent: **Rc** siRNA without drug; **Cc** nontargeting siRNA without drug; **Cd** nontargeting siRNA with drug; **Rd** siRNA without drug. An average SI was calculated for each siRNA across triplicates following paclitaxel treatment. An individual siRNA target with an average SI > 0.1 was considered a synergistic effector with paclitaxel.

Transient knockdown

A mixture of 50 µL of Opti-MEM (Invitrogen, USA), 0.3 µL of Lipofectamine RNAiMAX Transfection Reagent (Thermo Fisher Scientific, USA) and 50 nM individual siRNA was preincubated in triplicate in 96-well plates. Cells were seeded in 100 µL of antibiotic-free DMEM containing 10% FBS (3000

cells/well). Target sequences of siRNA for transient knocking down SYTL4 were as follows: siRNA1: 5'-GCAGCATGATGAGCATCTA-3'; siRNA2: 5'-GTC TGGTTGCCATGTGAA-3'; siRNA3: 5'-GCTGGCCT ATGCTGATGAA-3'; siRNA4: 5'-GGATATGGAAGA GGAAGAA-3'; siRNA5: 5'-GGATTTGATTCTCAGT GTT-3'. Scrambled siRNA was used as a control. The siRNA transfection was conducted according to the manufacturer's protocol.

Plasmids, lentivirus infection and generation of stable cell lines

Target sequences of short hairpin RNA (shRNA) for stably knocking down SYTL4 were as follows: shNC: 5'-TTCTCCGAACGTGTCACGT-3'; shSYTL4-1: 5'-TCCCTTTACATGGAAAGAT-3'; shSYTL4-2: 5'-CCAAGGAAATAGAGTTGAA-3'.

Lentiviral plasmids containing the fragment of SYTL4, SYTL4-GFP, or three domains of SYTL4 fused with GFP at their C-terminus (D1/D2/D3-GFP) were constructed by inserting corresponding PCR product into the pCDH-CMV vector between BamHI and EcoRI sites. Constructs were examined by Sanger sequencing and selected for further experiments.

Using Lipofectamine 2000 transfection reagent (Thermo Fisher Scientific, USA), 293T cells were co-transfected with lentivirus vectors and packaging vectors (psPAX2 and pMD2.G). Viral supernatants were collected and filtered after 48 h. Cells infected by the lentivirus were subjected to puromycin selection. Alterations in the expression level were verified by western blot analysis.

Western blot analysis

Western blotting was performed as described previously [31]. Briefly, equal amounts of protein samples were resolved by SDS-PAGE and transferred to PVDF membranes (Roche, Switzerland). Blocking was performed with 5% skim milk, and blotting was performed with primary antibodies and secondary HRP-conjugated antibodies as indicated. The signal was detected by enhanced chemiluminescence substrate (Pierce Biotechnology, USA) under Tanon 4200. For quantification, the intensity of the western blot band was analyzed using Fiji (National Institutes of Health, USA).

Cell proliferation assay

For half maximal inhibitory concentration (IC₅₀) determination, cells (3×10^3 per well) were seeded in 96-well plates. After 24 h, the cells were treated with the indicated concentrations of drug or DMSO for an additional 3 days. Cytotoxicity was determined using the CCK-8 assay as described previously [31]. Briefly, the CCK-8 was prediluted with complete DMEM growth medium at 1:10, and 100 μ L solution was

added to each well. After incubation in 37 °C in the dark for 2-3 h, O.D values of plates were measured using a spectrometer at 450 nm. The IC₅₀ was determined according to a dose vs. response curve by GraphPad Prism 6.0.

For the *in vitro* cell growth assay, cells were seeded in 96-well plates and monitored using the IncuCyte ZOOM System (Essen BioScience, Germany). Images were captured at 12 h intervals from four separate regions per well. The relative survival rate was calculated by dividing the confluence of paclitaxel-treated cells by the confluence of DMSO-treated cells (%).

Colony-formation assay

Briefly, 3000 cells were plated in triplicate in 1 mL of complete growth medium in a 24-well plate. The following day, paclitaxel or an equal volume of DMSO was added to the medium. After 2 weeks, the colonies were stained with 0.5% methylene blue in 50% ethanol. Colonies larger than 9 pixels² (50 cells) were counted by the particle analysis plugin in Fiji (National Institutes of Health, USA). The relative colony-forming efficiency was calculated by dividing the number of paclitaxel-treated colonies by the number of DMSO-treated colonies (%).

Patient-derived organoid culture

Histologically diagnosed TNBC tissues were obtained from freshly resected specimens during surgery at FUSCC. Patients were informed before the surgery and agreed by written consent to tissue collection. Tissue processing, organoid culture and drug sensitivity test were performed as described previously [33, 34]. Tumors were processed immediately upon receipt and cultured as described below. These untrypsinized organoids were embedded in 30 or 80 μ L Matrigel depending on the tumor volume. After solidification of the Matrigel-cell solution in 24-well plates, breast cancer organoid medium was added immediately and changed every 4 days. Organoids were harvested for qRT-PCR analysis after 2 to 4 weeks. Organoids were trypsinized and passaged approximately every 14-21 d.

For lentiviral transduction in organoids, high titer virus was collected through ultracentrifugation at $50,000 \times g$ for 90 min, resuspended with 500 μ L of organoid culture medium supplemented with 8 μ g/mL polybrene and stored at -80 °C as described previously [35]. Organoids were split into new wells to obtain small organoids two days before transfection. On the day of transfection, organoids were harvested, trypsinized, resuspended with 20 μ L of medium, and mixed with 250 μ L of high titer

lentivirus. Then, the organoid-virus mixture was incubated in a 48-well plate for 3 hours at 37 °C, centrifuged, washed and seeded in a 48-well plate. Three days later, fresh medium with puromycin (4 µg/mL) was added. Organoids were selected by puromycin for 2 weeks and then were harvested for qRT-PCR analysis after 2-4 weeks.

For the drug sensitivity test, organoids were harvested and diluted to 75 organoids/µL in growth medium. Black, clear-bottom 384-well plates (Corning) were coated with 10 µL of basement membrane extract (BME) before the addition of 30 µL of organoid suspension. Then, six concentrations of paclitaxel, as well as the DMSO control, were added in triplicate. CellTiter-Glo 3D Reagent (Promega) was added after five days, and the plate was agitated on a shaker for 30 min at room temperature. The luminescence was measured with a SpectraMax microplate reader (Molecular Devices). Data were analyzed using GraphPad Prism 8.0, followed by the manual determination of the IC50 values.

Measurement of tubulin polymerization

Cells were grown in duplicate wells of 24-well plates to 80% confluence and remained untreated or treated overnight with 10 nM paclitaxel for 16 to 18 hours. The tubulin in microtubules was measured as described previously [36]. Briefly, the cells were lysed in a microtubule-stabilizing buffer, which contains 20 mM Tris-HCl (pH 6.8), 0.14 M NaCl, 0.5% NP40, 1 mM MgCl₂, 2 mM EGTA, and 4 µg/mL paclitaxel. The lysates were then centrifuged at 10,000 × *g* for 20 min to obtain the pellet fraction containing microtubules (*P*) and supernatant fraction containing soluble tubulin (*S*). Western blot analysis was performed using the indicated antibodies. The percentage of assembled tubulin was calculated as:

$$\frac{P}{P + S} \times 100 (\%)$$

Tubulin turbidity assay

The microtubule polymerization was monitored by measuring changes in absorbance (340 nm) by a spectrophotometer as described previously [37]. Briefly, all of the components of the reactions from the Tubulin Polymerization Assay Kit (Cytoskeleton, USA) were mixed in 96-well plates according to the manufacturer's protocol. After gentle mixing, the absorbances of the reaction mixtures were immediately determined by a spectrophotometer at 37 °C for 60 min.

Immunofluorescence imaging

Staining and imaging of monolayer cells were performed as described previously [31]. In detail, cells

grown on glass coverslips were first washed with 37 °C 1×PBS to avoid cold-induced depolymerization of microtubule. Then, 4% formaldehyde (in PBS) was used for fixation for 15 min at room temperature. Next, cells on coverslips were permeabilized by 0.25% TritonX-100, blocked with 5% BSA in 1×PBS, and then incubated with primary antibodies for 1 h at room temperature, which included mouse monoclonal anti-α-tubulin (Proteintech, USA) and rabbit polyclonal anti-SYTL4 (Proteintech, USA). After being incubated with appropriate fluorescent secondary antibodies (Invitrogen, USA) and washed, the nuclei were counterstained with DAPI (Sigma-Aldrich, USA). Finally, the glass coverslips were mounted onto glass slides with Fluoromount aqueous mounting medium (Sigma). Images were acquired and deconvolved using Deltavision Elite (GE, USA) or captured by an Olympus IX53 fluorescence microscope (Olympus Corporation, USA). For super-resolution images, slides were scanned by structured illumination microscopy (SIM) technology by DeltaVision OMX SR (GE Healthcare, USA).

Polymerized microtubules were evaluated by Fiji using the Tubeness plugin. Original images were converted into 8-bit format and followed by Tubeness analysis (sigma = 1.0) to select tubule-like structures. Then, images were converted into 8-bit format again and applied with the same threshold for comparison. Particle analysis was further used to determine the area of the microtubule network to the whole cell. The percentage (%) of polymerized microtubules was represented by the ratio of the area of tubule-like structure to the region inside the cell contour.

Live cell tracking of EB1 motion

EB1 is a microtubule end-binding protein that tracks the tips of growing microtubules. The EB1-ΔC-GFP construct [38] was synthesized (Genscript) and cloned into a lentiviral vector and then was stably expressed in cells by lentiviral transduction. For real-time tracking of EB1 motion, DeltaVision Elite imaging system was used with a 100× /1.40 NA Plan Apo oil-immersion objective (Olympus), and the CoolSnap HQ2 camera (Photometrics) equipped with the live cell imaging environment control system (Live Cell Instrument). Images were captured in 30 s with 14 intervals and deconvolved by the DeltaVision Elite software. The motion and speed of EB1 were analyzed by the particle tracking function in Imaris 9.0.

Coimmunoprecipitation

Cells grown in 10-cm dishes were washed once with 1×PBS and lysed with Western/IP lysis buffer (Beyotime, China) supplemented with 0.5 mM PMSF.

Following $12,000 \times g$ centrifugation at 4 °C for 5 min, the pellet containing the cell debris was removed, and the supernatant was harvested for Co-IP. Anti-GFP nanobody-coated agarose (KT health, China) was used according to the manufacturer's protocol. Briefly, cell lysate supernatant was mixed with anti-GFP nanobody suspension and incubated overnight on a rotator at 4 °C. The agarose beads were pelleted by centrifugation at $2,400 \times g$ for 1 min at 4 °C and washed three times with the Western/IP lysis buffer on ice. The beads were mixed with SDT lysis buffer (4% SDS, 100 mM DTT, 100 mM Tris HCl) for elution. Co-IP samples were analyzed by western blot assay.

Pull-down assay

Purified 6×His tag peptide or His-SYTL4 protein was incubated with tubulins and 50 µl of nickel-nitrilotriacetic acid (Ni²⁺-NTA) beads (Thermo Scientific, USA) in 500 µl of western/IP lysis buffer (Beyotime) at 4 °C overnight. Subsequently, the His pull-down products were washed three times. Laemmli buffer was used to elute the protein, which was further detected by western blot with anti-α-tubulin and anti-SYTL4 antibodies.

Orthotopic nude mouse models and treatment

To establish orthotopic models, MDA-MB-231 cells expressing shNC or shSYTL4 (5×10^6 cells) were resuspended in 50 µL of PBS and 50 µL of Matrigel (BD Biosciences, USA) and injected directly into mammary fat pads of 4-6-week-old female BALB/c nude mice. When the average tumor volumes were 50-100 mm³ after implantation, the mice bearing each cell line were randomly assigned to two groups, namely, the vehicle or paclitaxel group. Vehicle or paclitaxel (10 mg/kg) was administered by intraperitoneal injection every 2 days for 9 times. Three days after the last dose, the mice were sacrificed. Tumor volumes were calculated as $V = L \times W \times W / 2$, where L is the length (longest dimension) and W is the width (shortest dimension). A paired t test was performed to compare the tumor volumes between groups. The animal study protocol was approved by the Animal Ethics Committee of the Fudan University.

Immunohistochemistry staining

Immunohistochemistry (IHC) was performed and evaluated using a two-step method as described previously [39]. Immunostaining was performed on the TNBC cohort C using tissue microarrays (TMAs). A rabbit polyclonal antibody against SYTL4 (Abcam, USA) was applied to the TMAs. IHC staining of SYTL4 was mainly found in the cytoplasm of tumor cells. For the quantification of SYTL4 expression, both

the staining intensity and the percentage of stained cells were evaluated as the histological score (H-score) [39]. For statistical analysis, H-scores (ranging from 0-12) of 0 to 7 were considered low expression and scores of 8 to 12 considered high expression.

Statistical analysis

All numerical data are expressed as the mean ± SD. The data were analyzed using a two-sided Student's *t*-test or a one-way ANOVA test. Comparisons of tumor characteristics were performed using the χ^2 test. Survival curves were constructed using the Kaplan-Meier method, and the univariate survival difference was determined with the log-rank test. Unadjusted hazard ratios with 95% CIs were calculated using Cox proportional hazards models. All statistical analyses were performed using GraphPad Prism, version 7.0 (GraphPad Software, USA) or Stata statistical software, version 14.1 (StataCorp, USA). A two-sided *P* < 0.05 was considered significant. * *P* < 0.05; ** *P* < 0.01; *** *P* < 0.001.

Further details are shown in the supplementary material.

Results

Identification of chemoresistance-related genes in TNBC under neoadjuvant chemotherapy

First, 8 patients with TNBC who underwent neoadjuvant paclitaxel and carboplatin regimen were divided into resistant (*n* = 5) and sensitive (*n* = 3) groups according to their response (Table S1). We next sequenced 10 tumor samples obtained from these eight patients by RNA-seq (Figure 1A). These 10 TNBC samples were classified into the following groups: pre-NAC resistant (*n* = 5); pre-NAC sensitive (*n* = 3); and post-NAC residual (*n* = 2). Compared with pre-NAC sensitive samples, 1,852 genes were upregulated in the pre-NAC resistant samples, of which enriched pathways are shown in Figure S1A-B. In all, 1,253 genes were highly expressed in both post-NAC residuals compared with pre-NAC resistant samples, and 18,11 genes were high in at least one patient (Table S2). Enriched pathways of these 1,253 genes are shown in Figure S1C-D. Common signatures between post-NAC residual versus pre-NAC resistant and pre-NAC resistant versus pre-NAC sensitive included epithelial mesenchymal transition (EMT), myogenesis, and angiogenesis. With regard to the KEGG collection, common signatures included focal adhesion, calcium signaling pathway, cAMP signaling pathway, ECM-receptor interaction, the PI3K-Akt signaling

pathway, and the Ras signaling pathway. To narrow down the gene numbers in the list for the next screening assay, we overlapped these genes and identified 434 common genes upregulated in both comparisons; these genes were enriched in ECM-receptor interactions, focal adhesion, PI3K-Akt signaling, and the regulation of actin cytoskeleton pathways (Figure 1B). These 434 genes may be predictive of response to paclitaxel and carboplatin combination therapy.

Because we only sequenced 10 NAC samples, we next applied a list of scoring standards to rank candidate genes (Supplementary Methods). One key standard is that the gene must be predictive of pCR in at least one public taxane-based NAC cohort. Thirty top genes were selected for further functional exploration (Figure 1C), including SYTL4, BCAM, CTPS2, FKBP9, LAMA3, PDGFRB, and ZNF160 (Table S3).

In vitro siRNA pool functional screen identified SYTL4 as a chemoresistant gene

Next, we performed an siRNA pool-based

screening of these above 30 genes. MDA-MB-231 cells (representing TNBC) were seeded, transfected, treated and measured using the CCK-8 assay (Figure 2A). The degree of paclitaxel sensitization calculated by SI equation across all targets distributed in a reverse S-shaped curve (Figure 2B). The top genes were ranked by the average SI (Figure 2C). Some reported chemoresistant genes, such as AHR [40] and SIK2 [41], were present as well, confirming the reliability of our screening method. SYTL4 had the highest average SI. The knockdown efficiency of siRNAs targeting SYTL4 in MDA-MB-231 cells was validated by qRT-PCR and western blot (Figure 2D). The relative SYTL4 expression was down to approximately 20% of baseline by siRNA2, with IC50 of paclitaxel being decreased by 2.8-fold (Figure 2E). Utilizing public data, we found a significant positive correlation between SYTL4 mRNA expression level and the IC50 value for paclitaxel (Pearson’s $R^2 = 0.71$, $P = 0.004$; Figure S2A) but not for vinorelbine (Pearson’s $R^2=0.33$, $P=0.108$; Figure S2B). The SYTL4 protein level was quantified by western blotting in another eight TNBC cell lines (Figure S2C).

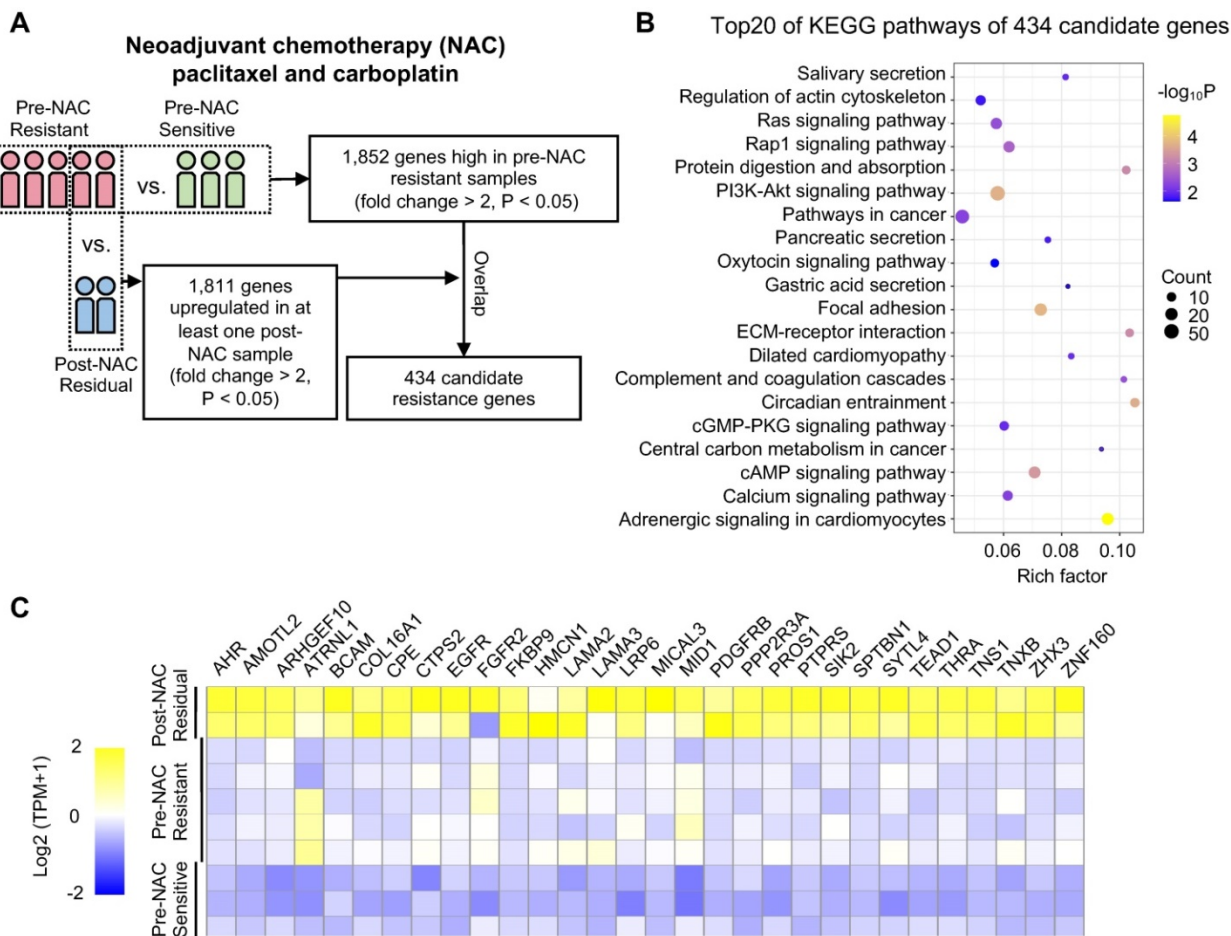


Figure 1. Procedure for selecting differentially expressed genes associated with chemoresistance. (A) Schematic diagram of overlapping candidate genes from RNA-seq data of triple-negative breast cancer (TNBC) samples that underwent neoadjuvant chemotherapy (NAC). **(B)** Top 20 of Kyoto Encyclopedia of Genes and Genomes (KEGG) pathways of 434 candidate genes as shown in (A). **(C)** Heatmap of the 30 top-ranked genes in 434 candidates above. The ranking standard was described in the methods.

Simultaneously, the paclitaxel sensitivity of each cell line was assessed. A positive correlation between SYTL4 expression and IC₅₀ value of paclitaxel was observed (Pearson's $R^2 = 0.90$, $P < 0.001$; Figure 2F). Given that SYTL4 was identified from patients treated with both paclitaxel and carboplatin, we also assessed the role of SYTL4 in carboplatin sensitivity. As shown in Figure S2D, knocking down SYTL4 did not alter the carboplatin sensitivity of MDA-MB-231 cells. The synergy scores of carboplatin combined with

paclitaxel were calculated by SynergyFinder 2.0 [42]. Knocking down SYTL4 did not alter the additive interaction between these two drugs in MDA-MB-231 cells (Figure S2E). Of note, silencing SYTL4 did not alter the sensitivity of MDA-MB-231 cells to other nontaxane drugs-vinorelbine (a microtubule-destabilizing agent) or doxorubicin (a DNA-damaging agent) (Figure S2F). We thus chose SYTL4 as the leading potential candidate for paclitaxel resistance in further exploration.

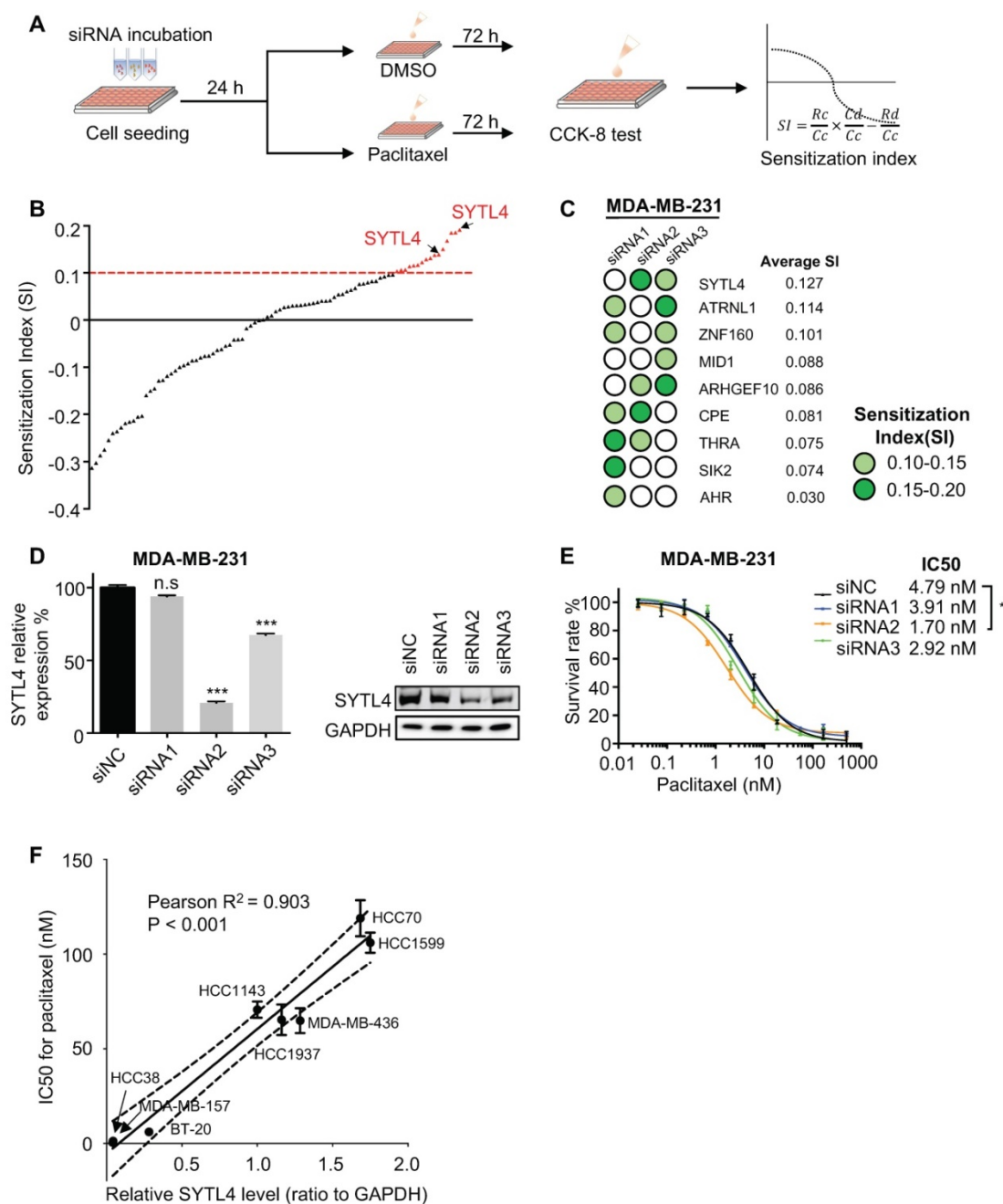


Figure 2. Functional screening based on an siRNA pool assay in MDA-MB-231 cells. (A) Schematic diagram of the siRNA-based screening. Sensitization index (SI) was described in the Methods section. Higher SI indicates a higher synergistic effect of siRNA with paclitaxel. (B) Sensitization index (SI) distribution curve. Dots in red: siRNA targets with SI > 0.1. (C) Average SI of three targets of genes from (B). (D) Relative gene expression of SYTL4 in MDA-MB-231 cells after siSYTL4 treatment. Left: qRT-PCR quantification of mRNA level (mean ± SD, n = 3). $2^{-\Delta\Delta Ct}$ was used and GAPDH was set as the inner control. Right: western blot analysis of SYTL4 expression. (E) IC₅₀ of paclitaxel in MDA-MB-231 cells with siSYTL4 knockdown. Two-way ANOVA test was used to compare the effect of siRNA2 to siNC. (F) Correlation between relative SYTL4 protein level and IC₅₀ of paclitaxel in TNBC cells. Pearson's correlation R^2 was calculated and tested. SYTL4 protein level was estimated by quantification of the gray intensity of western blot bands as shown in Figure S2C. * $P < 0.05$; ** $P < 0.01$; *** $P < 0.001$; n.s: not significant.

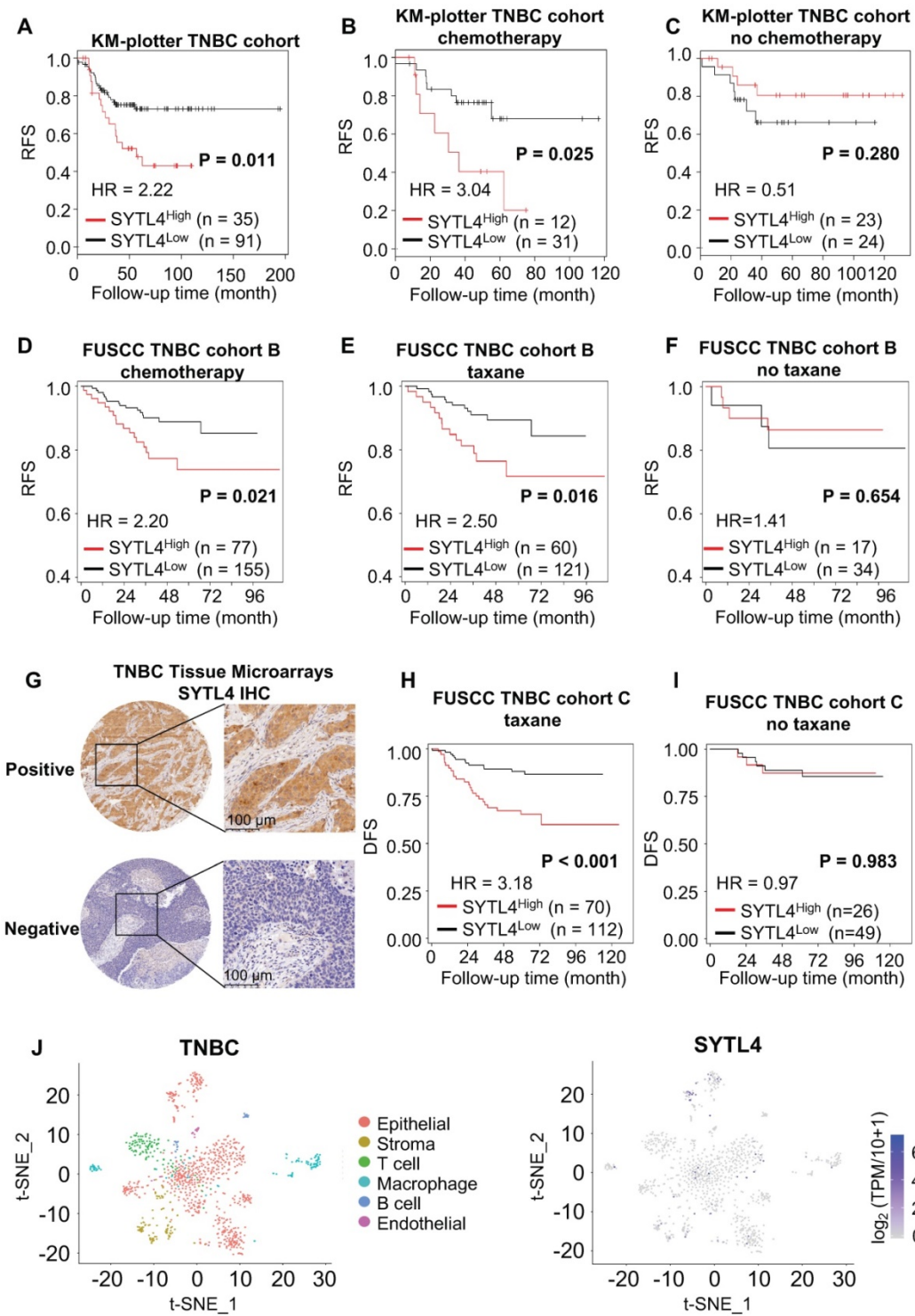


Figure 3. SYTL4 correlated with poor prognosis in taxane-treated TNBC cohorts. (A–C) Survival analysis of SYTL4 expression in TNBC cohort from KM-plotter [43]. **(D–F)** Survival analysis of SYTL4 expression in FUSCC TNBC cohort B (n = 232). **(G)** Representative images of SYTL4 expression in tumor tissue microarrays of TNBC by IHC. **(H, I)** Survival analysis of SYTL4 protein level and in FUSCC TNBC cohort C (n = 182). SYTL4 protein level was estimated by IHC as described in the Methods section. **(J)** t-SNE plot of all 1,069 classified TNBC cells, demonstrating separation of cells by cell type (left panel). Expression level and distribution of SYTL4 vary across cells (right panel). The hazard ratio (HR) was calculated by univariate Cox regression. DFS, disease-free survival; FUSCC, Fudan University Shanghai Cancer Center; IHC, immunohistochemistry; RFS, recurrence-free survival; TNBC, triple-negative breast cancer; t-SNE, t-distributed stochastic neighbor embedding.

The prognostic value and clinical relevance of SYTL4 in TNBC

We next assessed the prognostic value of SYTL4 in TNBC. In a public TNBC cohort from KM-plotter

[43], high SYTL4 expression showed worse recurrence-free survival (RFS) in the full TNBC set (hazard ratio [HR] = 2.22, P = 0.011; Figure 3A). The HR of SYTL4 expression increased to 3.04 in chemotherapy-treated TNBC (P = 0.025; Figure 3B). In

contrast, the prognostic value of SYTL4 mRNA was not significant in the subset without chemotherapy (Figure 3C). Additionally, in our FUSCC TNBC cohort B [5], a high level of SYTL4 mRNA indicated worse RFS in 232 TNBC cases who received adjuvant chemotherapy (HR = 2.20, $P = 0.043$; Figure 3D), specifically in taxane-treated patients (HR = 2.50, $P = 0.027$; Figure 3E) but not in those without taxane treatment (Figure 3F). Tumors with high levels of SYTL4 were enriched in MES subtypes ($P = 0.001$; Table 1) and enriched in myogenesis, EMT, apical junction and angiogenesis signatures by GSEA (Table S4). The protein level of SYTL4 in TNBC was evaluated by IHC on TMAs in another TNBC cohort (Figure 3G). High protein level of SYTL4 significantly correlated with poor disease-free survival (DFS) in taxane-treated patients (HR = 3.18, $P < 0.001$; Figure 3H), but not in those without taxane treatment ($P = 0.983$; Figure 3I). These results indicated SYTL4 as a poor prognostic indicator for taxane-treated TNBCs.

We next compared the mRNA expression of SYTL4 between 1) pre-NAC samples from pCR ($n = 12$) and non-pCR patients ($n = 12$) and 2) pre- and post- NAC samples from non-pCR patients ($n = 12$) in a TNBC cohort that underwent taxane-containing NAC. TNBC patients who did not reach a pCR had a significantly higher level of SYTL4 expression ($P < 0.001$; Figure S3A). After NAC, the SYTL4 mRNA level increased at 1.2- to 3-fold after NAC in approximately 75% of non-pCR patients ($P < 0.01$; Figure S3B). Within public breast cancer cohorts that underwent NAC, SYTL4 was also highly expressed in non-pCR patients (GSE22513) and upregulated in post-NAC samples (GSE32603) (Figure S3C-D). These results validated the reliability of SYTL4 in NAC samples.

Since single-cell sequencing helps identify intratumor heterogeneity of breast cancer, we explored the distribution of SYTL4 expression utilizing single-cell data of TNBC [44]. SYTL4 was highly expressed in a cluster of epithelial tumor cells (Figure 3J), which were enriched in metabolic-related pathways (Table S5).

In summary, these data suggested that highly expressed SYTL4 indicated poor prognosis and chemotherapy response in TNBC patients.

SYTL4 promoted paclitaxel resistance in TNBC *in vitro* and *in vivo*

To explore the phenotype of SYTL4-mediated resistance *in vitro* and *in vivo*, we first evaluated SYTL4 expression across breast cancer cell lines in publicly available data (GSE58135). SYTL4 was highly expressed in most ER-positive and HER2-positive cells (Figure S4A). Protein SYTL4 expression was

similar to its mRNA expression pattern (Figure S4B). In tumors, the SYTL4 mRNA level was significantly lower in the basal-like subtype than luminal-like ones within The Cancer Genome Atlas (TCGA) cohort. However, within the FUSCC TNBC cohort, SYTL4 was expressed highly in the MES subtype, a subtype possessing the poorest survival [5] (Figure S4C), suggesting a distinct role of this protein in TNBCs.

We stably silenced SYTL4 expression through short hairpin RNA (shRNA) in MDA-MB-231 and Hs578T cells, two TNBC cell lines. Western blot analysis showed that shRNA target 2 worked well in both cell lines (Figure 4A).

As expected, the IC50 value in shSYTL4-2 cells (hereafter referred to as shSYTL4) was approximately 5-fold lower in MDA-MB-231 cells and 7-fold lower in Hs578T cells compared with shNC cells (Figure 4B). We also performed IC50 assays in MDA-MB-231 cells utilizing another two working siRNAs targeting SYTL4 (Figure S5A). Knocking down SYTL4 decreased IC50 values significantly (Figure S5B). Consistent with this finding, colony-formation assays (Figure 4C) and proliferation assays (Figure 4D) showed that SYTL4 knockdown significantly improved sensitivity to paclitaxel without affecting cell proliferation in both cell lines. Rescuing SYTL4 expression in MDA-MB-231-shSYTL4 cells improved the IC50 value to an equivalent level in MDA-MB-231-shNC cells (Figure 4E). In addition, over-expressing SYTL4 increased the resistance of MDA-MB-231 and Hs578T cells more resistant to paclitaxel (Figure S5C-H). Furthermore, silencing SYTL4 enhanced sensitivity to paclitaxel in the BALB/c nude mouse model (Figure 4F) without affecting tumor growth (Figure S6A-B). These data indicated that altering the SYTL4 level could affect the sensitivity of TNBC cells to paclitaxel *in vitro* and *in vivo*.

Patient-derived organoids (PDO) is a reliable model reflecting the chemosensitivity of individual patients [34]. Hoechst/PI staining showed that treating PDO with paclitaxel induced evident apoptosis (Figure S6C). SYTL4 high-expression TNBC organoids were more resistant to paclitaxel (Figure 4G-H). Meanwhile, knocking down SYTL4 in organoids improved the tumor sensitivity to paclitaxel (Figure 4I-J), suggesting that SYTL4 may serve as a potential therapeutic target for paclitaxel resistance in TNBC.

Altogether, *in vitro* and *in vivo* models validated that SYTL4 promoted paclitaxel resistance in TNBC.

SYTL4 interacted with microtubules

According to COMPARTMENTS Experimental Protein Localization Evidence Scores, SYTL4 is one of the 494 proteins localized to the microtubule

cytoskeleton [45, 46]. We thus visualized the distribution of SYTL4 by deconvolution-based fluorescence microscopy (Figure 5A). SYTL4 colocalized with α -tubulin, as indicated by the Pearson's correlation (Figure 5B). Of note, MDA-MB-231 cells with SYTL4 knockdown showed specific loss of staining by immunofluorescence (Figure S7A-B), confirming antibody specificity for SYTL4. Furthermore, live-cell imaging in MDA-MB-231 cells showed the colocalization between SYTL4-RFP and microtubules (Figure S8A-B). In addition, the SYTL4-tubulin complex could be coimmunoprecipitated (co-IP) in cell lysates (Figure 5C-D), suggesting their interaction. Finally, we questioned which domain of SYTL4 was responsible for this interaction. Three parts of SYTL4, the SHD domain (D1), the linker-C2A domain (D2) and the C2B domain (D3), were overexpressed in 293T cells individually as D1-GFP, D2-GFP, and D3-GFP (Figure 5E). Super-resolution imaging analysis through structured illumination microscopy (SIM) suggested that D2 attached to the surface of microtubules, while D1 exhibited a freely distributed pattern and D3 specifically localized near the plasma membrane (PM) (Figure 5E). Consistent with this finding, co-IP assay confirmed that D2 was responsible for interacting with microtubules (Figure 5F). These data indicated that SYTL4 interacted with microtubules through the region containing the linker-C2A domain.

SYTL4 induces microtubule instability in TNBC cells

Paclitaxel-induced cytotoxicity depends primarily on stabilizing microtubules [47]. Enhanced paclitaxel sensitivity could arise from enhanced microtubule stability. Because SYTL4 interacted with microtubules, we questioned whether SYTL4 confers paclitaxel resistance by affecting microtubule stability. The state of tubulin acetylation (ace-tubulin), a marker for stable microtubules [48], was detected by western blot. The data showed that SYTL4 knockdown increased the acetylation levels of tubulin in both MDA-MB-231 and Hs578T cells with or without paclitaxel treatment (Figure 6A). In addition, overexpressing SYTL4 decreased the level of acetylated tubulin to 50% in MDA-MB-231 and Hs578T cells (Figure S8C). Percentages of intracellular polymerized tubulin in both MDA-MB-231 and Hs578T cells were quantified. We found that stable microtubule (P) was significantly increased after knocking down SYTL4 with or without paclitaxel treatment (Figure 6B). Furthermore, SYTL4 knockdown also stabilized microtubules against cold treatment, a microtubule depolymerization inducer (Figure 6C). Another two siRNAs targeting SYTL4

(siRNA4 and siRNA5) validated this phenotype (Figure S9A-B).

Table 1. Correlation between clinicopathologic characteristics and SYTL4 mRNA expression in FUSCC TNBC cohort B

	SYTL4 low, n = 155 (%)	SYTL4 high, n = 77 (%)	P-value
Median follow-up (IQR) (mo)	40.8 (34.1-59.6)		-
Age			
18-49	58 (37.4)	29 (37.7)	0.971
≥50	97 (62.6)	48 (62.3)	
Menopause			
Yes	102 (65.8)	45 (58.4)	0.541
No	51 (32.9)	31 (40.3)	
N/A	2 (1.3)	1 (1.3)	
Grade			
2	18 (11.6)	11 (14.3)	0.387
3	126 (81.3)	57 (74.0)	
N/A	11 (7.1)	9 (11.7)	
T stage			
T1	53 (34.2)	28 (36.4)	0.744
T2-3	102 (65.8)	49 (63.6)	
LN status			
Negative	94 (60.6)	46 (59.7)	0.765
Positive	61 (39.4)	31 (40.3)	
Surgery			
BCS	3 (1.9)	1 (1.3)	0.220
Mastectomy	152 (98.1)	76 (98.7)	
Radiotherapy			
No	109 (70.3)	51 (66.2)	0.526
Yes	46 (29.7)	26 (33.8)	
FUSCC subtype			
BLIS	64 (41.3)	21 (27.3)	0.001
IM	43 (27.7)	14 (18.2)	
LAR	33 (21.3)	21 (27.3)	
MES	15 (9.7)	21 (27.3)	
Mutation subtype			
Aging	27 (17.4)	11 (14.3)	0.911
HRD	36 (23.2)	18 (23.4)	
MMR	16 (10.3)	10 (13.0)	
Mixed	22 (14.2)	9 (11.7)	
N/A	54 (34.8)	29 (37.7)	
sTIL group			
Low	112 (72.3)	60 (77.9)	0.347
High	17 (11.0)	4 (5.2)	
N/A	26 (16.8)	13 (16.9)	
iTIL group			
Low	69 (44.5)	33 (42.9)	0.968
High	60 (38.7)	31 (40.3)	
N/A	26 (16.8)	13 (16.9)	
Fibrosis			
0-2	100 (64.5)	48 (62.3)	0.064
3	13 (8.4)	14 (18.2)	
N/A	42 (27.1)	15 (19.5)	

Abbreviations: BCS, Breast Conserving Surgery; FUSCC, Fudan University Shanghai Cancer Center; HRD, Homologous Recombination Deficiency; IQR, Interquartile Range; iTIL, Intratumoral Tumor-infiltrating Lymphocyte; LN, Lymph Node; MMR, Mismatch Repair; N/A, Not Available; sTIL, Stromal Tumor-infiltrating Lymphocyte.

EB1- Δ C-GFP, the fluorescently labeled microtubule plus-end tracking protein, has become a practical tool for monitoring microtubule dynamics in live cells [38]. EB1- Δ C binds to the plus ends of microtubule as a "comet," which enables the quantification of microtubule growth rate. To assess the effects of SYTL4 on microtubule dynamics, we monitored over 15,000 EB1 tracks in control, SYTL4-

knockdown and SYTL4-overexpressing MDA-MB-231 cells (Figure 7A). We observed a trend, though not a significant one, for decreased the growth rates of tracks after knocking down SYTL4 ($P = 0.051$, Figure 7B). Growth rates of tracks after paclitaxel treatment further revealed that SYTL4 knockdown significantly decreased the microtubule growth rate of all tracks ($8.78 \pm 0.12 \mu\text{m}/\text{min}$ vs. $9.64 \pm 0.12 \mu\text{m}/\text{min}$; Figure

7B) and per cell means (Figure 7C). After SYTL4 overexpression, we observed a significant increase in the growth rate of all tracks ($10.59 \pm 0.09 \mu\text{m}/\text{min}$ vs. $9.59 \pm 0.10 \mu\text{m}/\text{min}$; Figure 7B) and the per cell means (Figure 7C). Taken together, these data indicated that SYTL4 increased dynamic instability during microtubule growth.

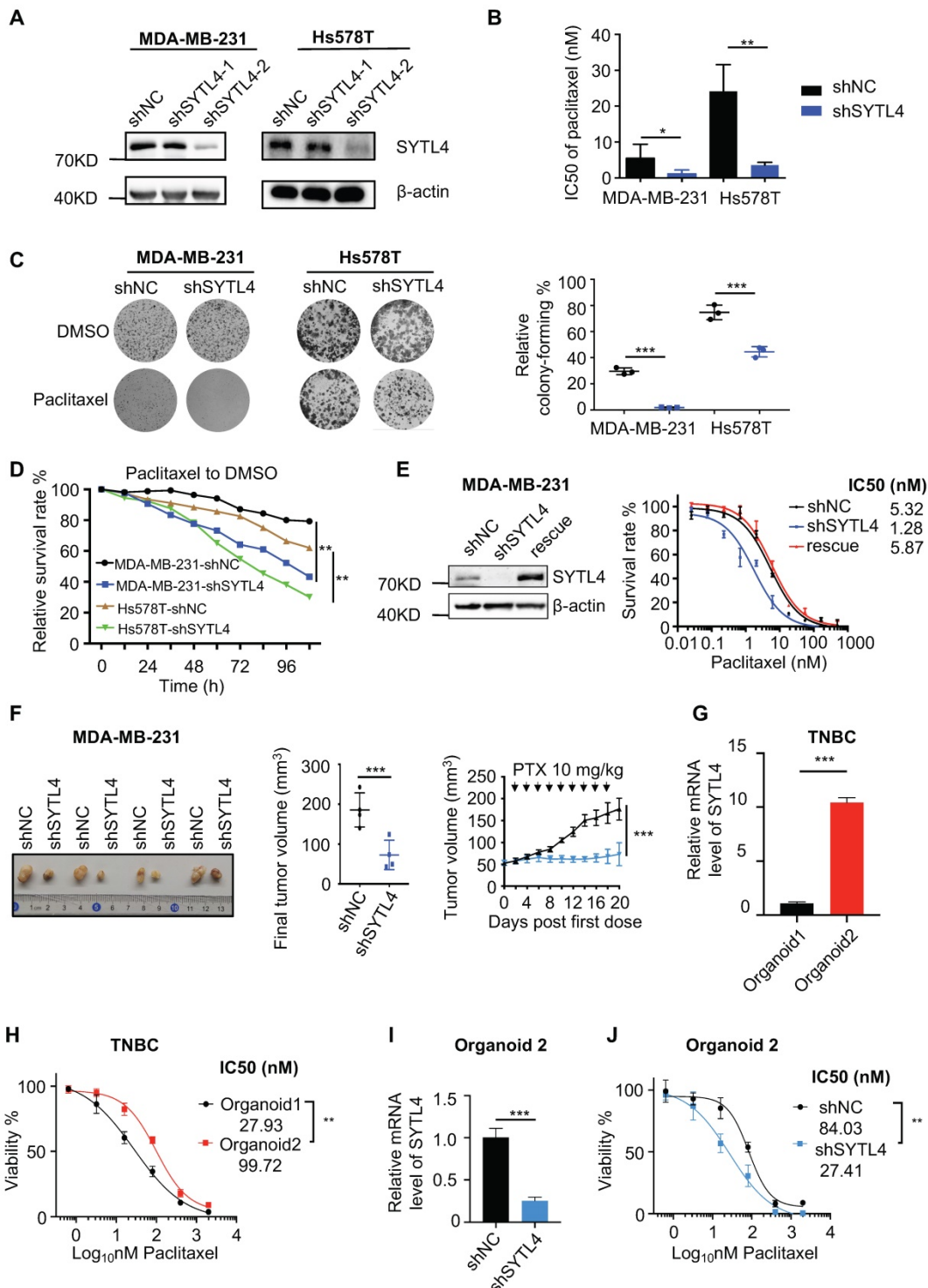


Figure 4. Knocking down SYTL4 increased the paclitaxel sensitivity in TNBC. (A) Western blot analysis of SYTL4 expression in MDA-MB-231 and Hs578T cells. The two short hairpin RNA (shRNA) target sequences were described in the Methods section. (B) IC50 of paclitaxel in cells with SYTL4 knockdown tested by the CCK-8 assay. The

data represents three independent assays (mean \pm SD, n = 3). (C) SYTL4 knockdown inhibited the cell colony-formation of MDA-MB-231 and Hs578T cells under paclitaxel treatment (1 nM). The relative survival rate was calculated by dividing colony numbers under paclitaxel treatment into colony numbers under DMSO. The data represent three independent assays (right) (mean \pm SD, n = 3). (D) IncuCyte-based real-time imaging analysis of cell growth with the treatment of paclitaxel. The relative cell survival rate on the Y axis was calculated by dividing the cell numbers under paclitaxel treatment by the cell numbers under DMSO treatment. (E) Rescuing SYTL4 expression increased the IC50 of paclitaxel in MDA-MB-231. Western blot analysis of SYTL4 expression (left). IC50 of paclitaxel in MDA-MB-231 (right). (F) SYTL4 knockdown inhibited tumor growth in nude mice after sequential paclitaxel (PTX) treatment. MDA-MB-231 cells with shNC or shSYTL4 were transplanted into nude mouse mammary fat pads in pairs as described in the Methods section. Arrows represent paclitaxel (10 mg/kg) treatment in tumor-bearing mice. Final tumor images were shown (left). Final tumor volume was calculated (middle) (mean \pm SD, n = 4) and tested by paired t test. *In vivo* growth curves quantified by tumor volume were illustrated (right) and tested by two-way ANOVA test. (G) qRT-PCR analysis of the relative mRNA levels of two TNBC organoids and tested by unpaired t test (mean \pm SD, n = 3). Human 18S rRNA was chosen as the reference gene. (H) Dose-response curves of organoid 1 (SYTL4 low expression) and organoid 2 (SYTL4 high expression) (mean \pm SD, n = 3, two-way ANOVA test). (I) qRT-PCR analysis of the relative mRNA levels of TNBC organoid 2 with shNC or shSYTL4 and tested by unpaired t test (mean \pm SD, n = 3). (J) Dose-response curves of organoid 2 (shNC vs. shSYTL4) (mean \pm SD, n = 3, two-way ANOVA test). * P < 0.05; ** P < 0.01; *** P < 0.001; n.s.: not significant.

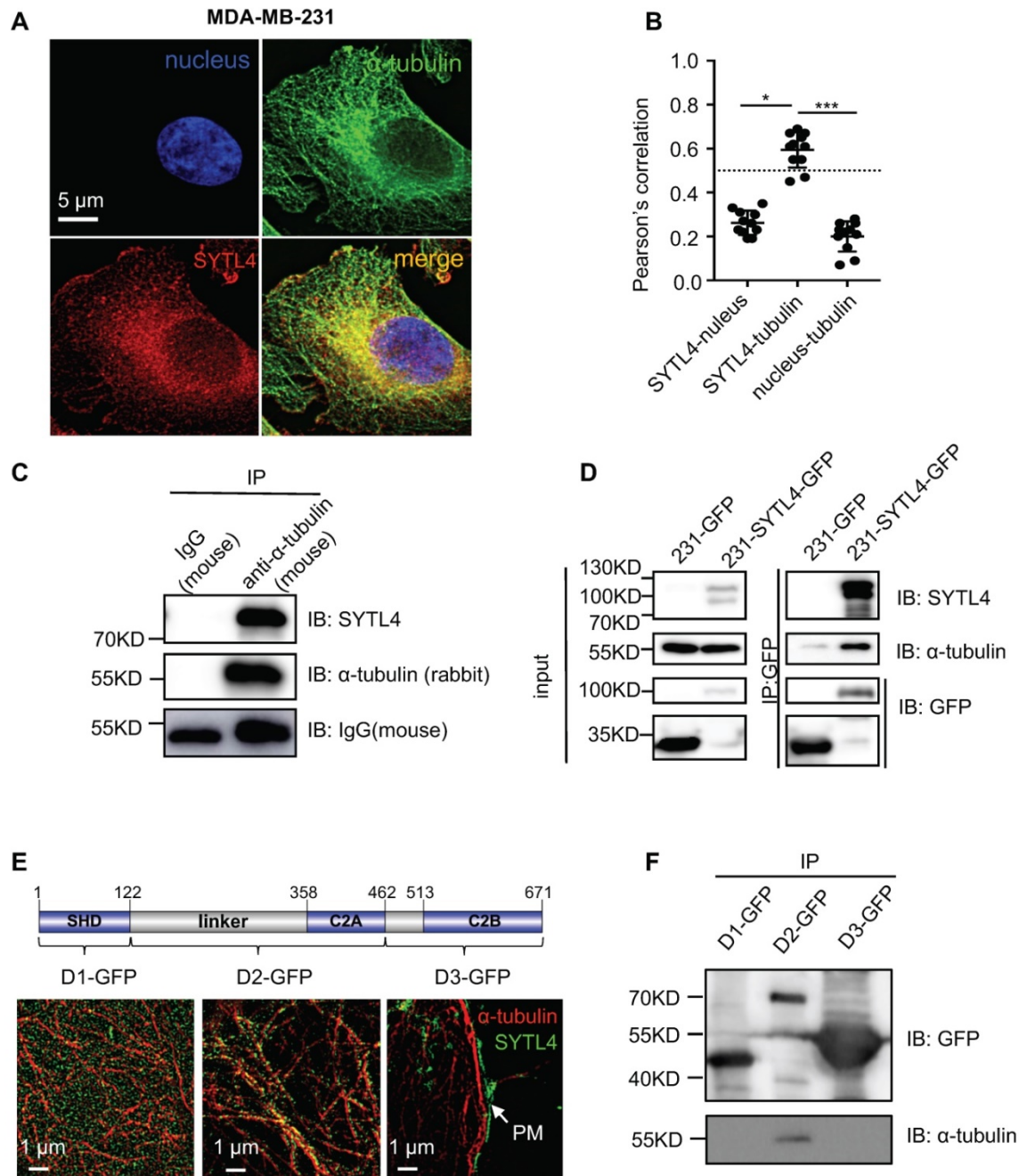


Figure 5. SYTL4 colocalized and interacted with microtubules. (A) SYTL4 colocalized with microtubules in MDA-MB-231 cells. Anti-SYTL4 and anti- α -tubulin antibodies were used and are described in the Methods section. Nuclei were stained by DAPI. Images were captured and deconvolved by DeltaVision microscopy. (B) Colocalization analysis by Pearson's correlation. The colocalization of SYTL4 and α -tubulin as shown in (A) was estimated by calculating the Pearson's correlation of their fluorescence intensities. The data represents the mean \pm SD estimated in at least 10 cells. (C) Coimmunoprecipitation (Co-IP) analysis of SYTL4-overexpressing MDA-MB-231 cells using anti- α -tubulin antibody. (D) Co-IP analysis of SYTL4-GFP-overexpressing MDA-MB-231 cells using anti-GFP nanobody-coated agarose beads. (E) Colocalization analysis of D1, D2 and D3 with microtubule by structured illumination microscopy (SIM) 293T cells. PM: plasma membrane. (F) Co-IP analysis of the interaction between SYTL4 D1, D2, D3 and microtubule. Co-IP assay was performed in 293T cells using anti-GFP beads. * P < 0.05; ** P < 0.01; *** P < 0.001; n.s.: not significant.

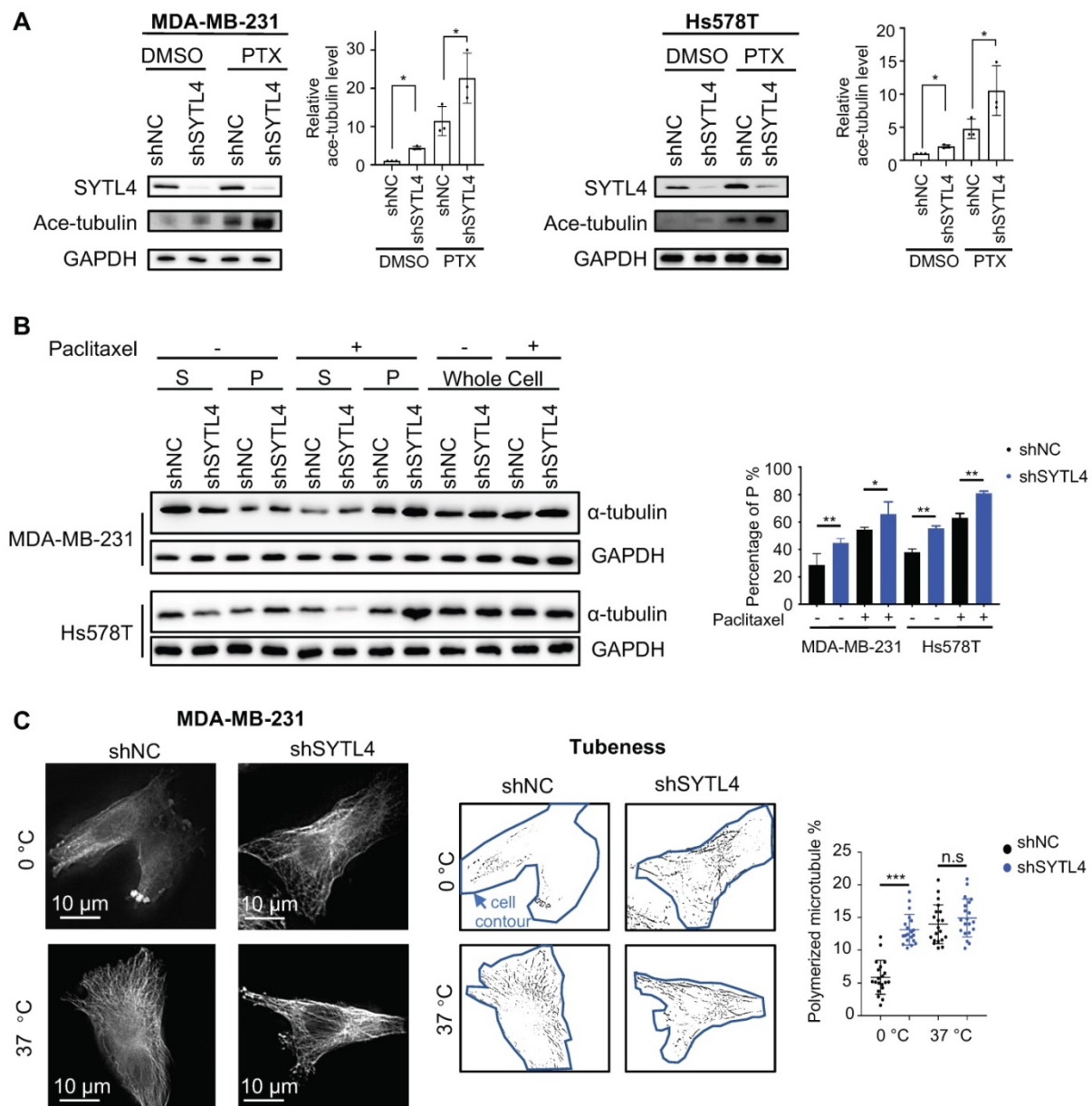


Figure 6. Knocking down SYTL4 enhanced microtubule stability in TNBC. (A) Western blot analysis of microtubule acetylation in MDA-MB-231 and Hs578T cells with or without PTX (paclitaxel) treatment. Band intensity was estimated by Fiji. The data represent the band intensity of ace-tubulin relative to the baseline intensity level of shNC cells under DMSO treatment (mean ± SD, n = 3, one-way ANOVA test). GAPDH was used for normalization. (B) Western blot analysis of microtubule stability in MDA-MB-231 and Hs578T cells (left panel). The lysates were separated into pellet fractions (P) containing microtubules and supernatant fractions (S) containing soluble tubulin. The band intensity was estimated by Fiji. The percentage of assembled tubulin was calculated as follows: $P/(P + S) \times 100(\%)$. The data represent the mean ± SD of three independent assays (one-way ANOVA test, right panel). (C) Immunofluorescence analysis of microtubule stability in MDA-MB-231 cells at 0 °C and 37 °C (left). Tubule-like structures were recognized by Fiji using the Tubeness plugin (middle) as described in methods. The percentage (%) of polymerized microtubules was calculated by dividing the area of tubule-like structure into the region inside the cell contour (right) (mean ± SD, n = 20, one-way ANOVA test). * P < 0.05; ** P < 0.01; *** P < 0.001; n.s: not significant.

The direct interaction between α-tubulin and SYTL4 was further validated by an *in-vitro* pull-down assay (Figure 7D). To determine whether SYTL4 could counteract microtubule polymerization, we conducted an *in vitro* microtubule polymerization assay. As a positive control, paclitaxel enhanced microtubule polymerization. Compared to the negative control, SYTL4 inhibited *in vitro* microtubule polymerization (Figure 7E). Taken together, these results demonstrated that SYTL4 increased the dynamic instability of microtubule polymers and thus

counteracted the microtubule polymerization effect induced by paclitaxel (Figure 8).

Discussion

Resistance to paclitaxel is a major obstacle to the acquired successful treatment of TNBC. Tumor tissue during NAC offers a great source of material for the identification of molecular markers associated with potential chemoresistance-associated alterations. However, tumors after chemotherapy are often paucicellular and contaminated with nontumor cells. To

overcome this limitation, we used post-NAC samples from patients with progressive disease, where tumor cells have outgrown nontumor cells. Previous molecular profiling of chemotherapy-resistant breast cancers has identified Ras-ERK pathway activation, degradation of ECM, AKT1 signaling via mTOR, hypoxia, EMT, and angiogenesis as activated pathways related to chemoresistance [15, 16, 18]. Similarly, we also identified the PI3K-Akt signaling pathway, the Ras signaling pathway, EMT, and angiogenesis. Coupled with functional screening *in vitro*, we report here that SYTL4 may be useful as a

biomarker of paclitaxel resistance.

We observed that SYTL4 expression was higher in post-NAC residual samples, suggesting that this upregulated expression arises from the *in vivo* drug selection of treatment-refractory subpopulations or drug stimulation in response to chemotherapy [18, 49]. Interestingly, we found that a low concentration of paclitaxel treatment did not alter SYTL4 expression in TNBC cells (data not shown). Future investigation is needed to determine why SYTL4 is highly expressed in chemoresistant TNBC tumors.

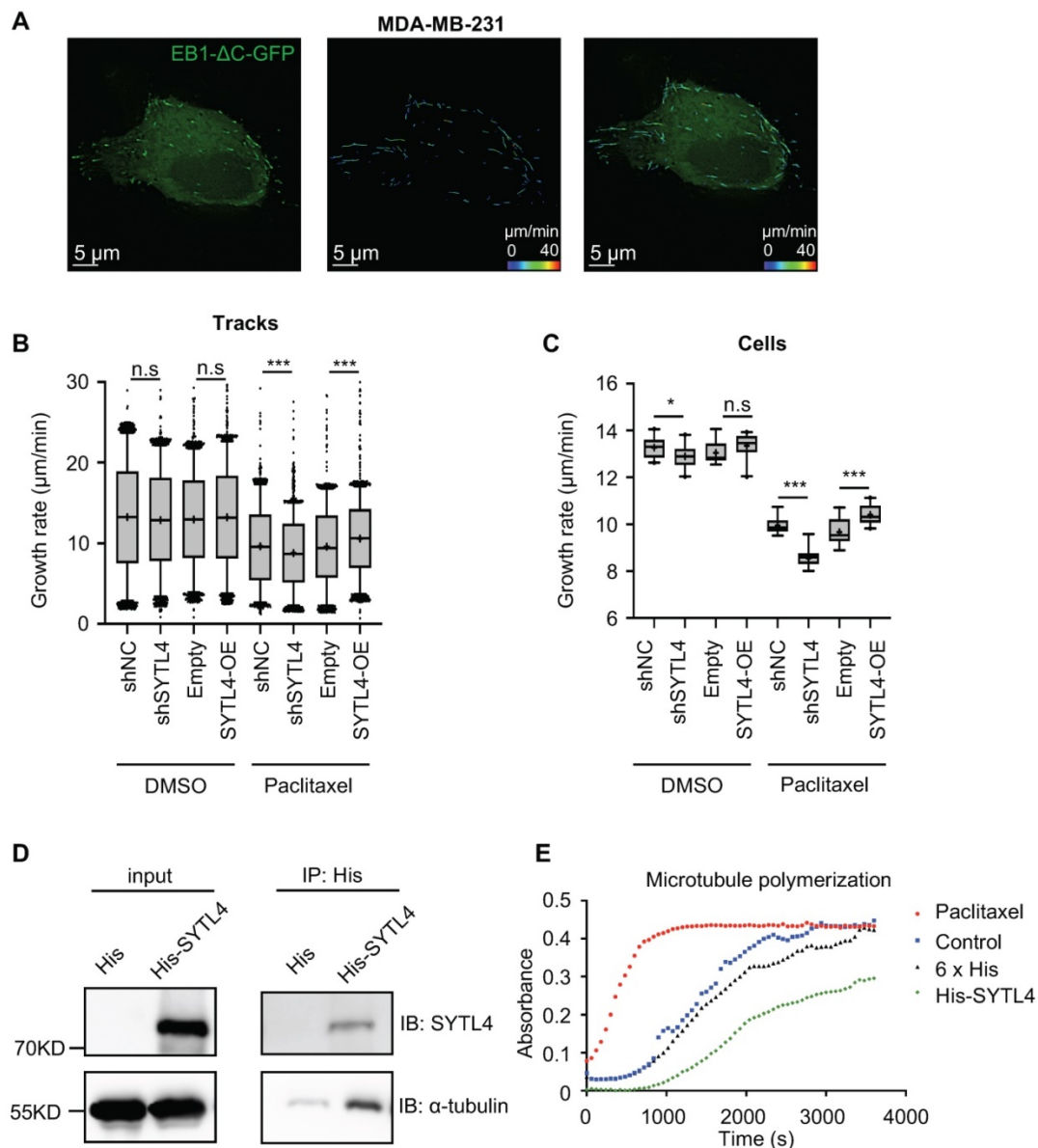


Figure 7. SYTL4 increased microtubule dynamics via directly destabilizing microtubule polymers in TNBC. (A) Representative image of EB1 comets and track overlays in an MDA-MB-231 cell. This image is a snapshot from a 30 s time-lapse recording (scale bar, 5 μm). Spectrum lines represented overall EB1-ΔC-GFP comet movement for a 30-s time-lapse recording. Time-lapse images were acquired every 2 s for 30 s. See the Methods for a more thorough explanation. **(B)** Growth rates of tracks with or without paclitaxel treatment in MDA-MB-231 cells. Microtubule growth rates were calculated by directly observing the EB1-ΔC-GFP comets. Box plots indicate the 5th percentile (bottom boundary), median (middle line), 95th percentile (top boundary) and mean value (+). Points represent outliers. One-way ANOVA test. **(C)** Growth rates per cell means with or without paclitaxel treatment in MDA-MB-231 cells. Box plots indicate the 5th percentile (bottom boundary), median (middle line), 95th percentile (top boundary) and mean value (+) (n = 20 cells per condition). One-way ANOVA test. **(D)** SYTL4 directly interacted with α-tubulin. A pull-down assay was performed in a mixture of purified His-SYTL4 protein and tubulin as described in the Methods section. **(E)** SYTL4 inhibited *in vitro* microtubule polymerization. Paclitaxel was used as a positive control, and 6x His was used as a negative control. His-tagged SYTL4 was added to the microtubule polymerization solution.

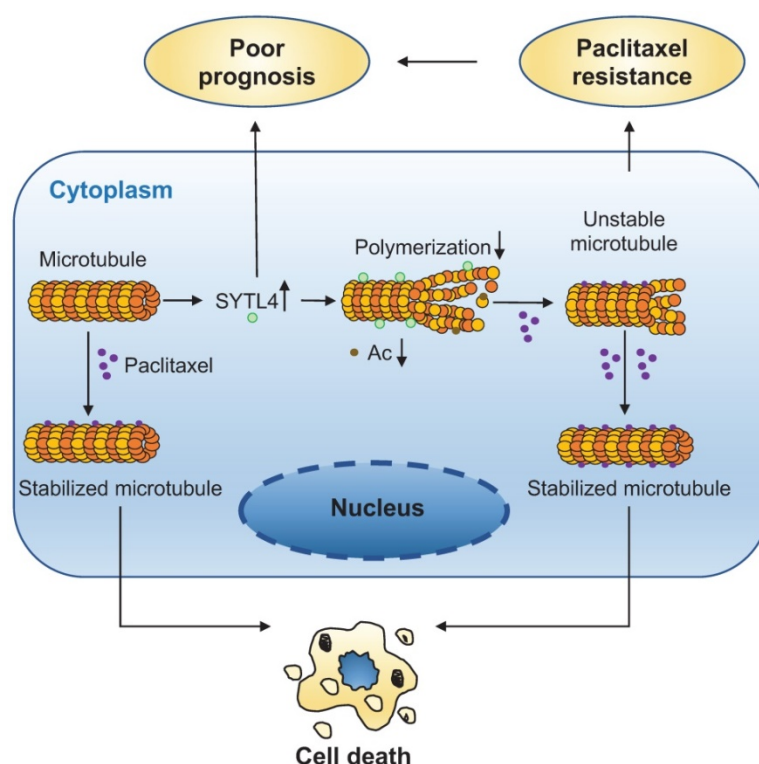


Figure 8. A schematic diagram for explaining the role of SYTL4 in conferring paclitaxel resistance in TNBC. Upregulated SYTL4 expression is correlated with poor prognosis in triple-negative breast cancer (TNBC). SYTL4 directly interacts with microtubules and inhibits the microtubule polymerization, thus increasing microtubule instability. Accordingly, the acetylation level (Ac) of microtubules decreases. Unstable microtubules require higher paclitaxel concentrations to keep stabilized and induce cell death, thereby mediating TNBC paclitaxel resistance.

Our data have several clinical implications. First, the level of SYTL4 correlated with poor prognosis and taxane response in TNBC, providing a new diagnostic marker for the administration of chemotherapy. Second, altering SYTL4 expression in MDA-MB-231 cells did not change its sensitivity to nontaxane drugs, including vinorelbine, a vinca alkaloid that interferes with microtubule assembly [50]. Thus, nontaxane-based regimens may benefit the TNBC patients with high-level SYTL4 expression. Third, downregulating SYTL4 expression via siRNA/shRNA knockdown or other techniques may provide a novel strategy to combat paclitaxel resistance in TNBC patients.

We clearly demonstrated a function of SYTL4 in the resistance to paclitaxel in at least two types of TNBC cells. Silencing of SYTL4 renders TNBC cells sensitive to paclitaxel both *in vitro* and *in vivo*, especially in PDO models, providing a new strategy to enhance paclitaxel sensitivity. In addition, we revealed SYTL4 as a novel microtubule-binding protein that decreased microtubule stability by counteracting microtubule polymerization. Importantly, SYTL4 was both predictive of response to taxane-based neoadjuvant chemotherapy and prognostic in taxane-treated TNBCs, which may serve as a candidate marker for predicting taxane response in TNBC.

Microtubules are essential components for vesicle transport. In turn, several molecular motors and Rab effectors have been shown to modulate microtubule stability [51]. Several microtubule-destabilizers have been reported to induce paclitaxel resistance by increasing the microtubule instability [31, 36, 52]. As a Rab27 effector, SYTL4 was previously identified to localize on intracellular vesicles and dock secretory granules to the plasma membrane for secretion through interacting with Rab3, Rab8 and Rab27 family members by the N-terminal Slp homology domain (SHD) [53, 54]. In addition, the linker region could interact with Munc18-1, syntaxin-1a, and Stx3, and the C-terminal C2AB domain has phospholipid interaction sites [55, 56]. Previous studies have illustrated the interplay between SYTL4 and kinesin-1 in linking granules along the cytoskeleton [57, 58]. Our study explored the distribution of SYTL4 proteins in cells and showed that a proportion of SYTL4 proteins colocalized with microtubules. We showed that SYTL4 could directly interact with microtubules through its middle region containing linker and C2A domain. This interaction results in microtubule instability and decreases sensitivity to paclitaxel in TNBC.

One of the limitations of this study is that the initial gene-list was generated from a small sample

size for the RNA-seq. However, we performed complementary analyses utilizing multiple public cohorts as well as a functional screening to narrow down the gene list and further validated the reliability of SYTL4 in another NAC cohort with a larger sample size. In addition, high SYTL4 expression correlated with myogenesis, EMT, apical junction and angiogenesis, suggesting a possible role of SYTL4 in the tumor microenvironment, which needs further assessment. It would also be interesting to investigate why SYTL4 is highly expressed in TNBC tumors but not in other breast cancer subtypes.

In conclusion, we suggest SYTL4 as a robust prognostic marker in taxane-treated TNBC, which may help in the selection of proper therapy and thus improve patient outcomes. In addition, we identified SYTL4 as a new microtubule destabilizer, enabling a better understanding of the regulatory mechanisms of microtubule dynamics in cancer cells.

Abbreviations

TNBC: triple-negative breast cancer; SYTL4: synaptotagmin-like 4; FUSCC: Fudan University Shanghai Cancer Center; NAC: neoadjuvant chemotherapy; pCR: pathologic complete response; PD: progressed disease; SI: sensitization index; IHC: immunohistochemical; IC50: half maximal inhibitory concentration; HR: hazard ratio; DFS: disease-free survival; RFS: recurrence-free survival; qRT-PCR: quantitative real-time polymerase chain reaction.

Supplementary Material

Supplementary figures and tables.

<http://www.thno.org/v10p10940s1.pdf>

Acknowledgements

This work was supported by grants from the National Natural Science Foundation of China (81922048, 81874112, 81874113, 81572583 and 81502278), the Training Plan of Excellent Talents in Shanghai Municipality Health System (2017YQ038), the “Chen Guang” project supported by Shanghai Municipal Education Commission and Shanghai Education Development Foundation (17CG01), Shanghai Pujiang Program (18PJD007), the Training Plan of Excellent Talents of Fudan University Shanghai Cancer Center (YJYQ201602), the Municipal Project for Developing Emerging and Frontier Technology in Shanghai Hospitals (SHDC12010116), the Cooperation Project of Conquering Major Diseases in Shanghai Municipality Health System (2013ZYJB0302), the Innovation Team of Ministry of Education (IRT1223), the Shanghai Key Laboratory of Breast Cancer (12DZ2260100), and the Shanghai Sailing Program (19YF1409000). The funders had no

role in the study design, data collection and analysis, decision to publish, or preparation of the manuscript.

Authors' contributions

Xi-Yu Liu and Wang Jiang designed and performed the experiments, analyzed the data and wrote the original manuscript. Ding Ma helped perform part of the clinical analysis. Yun-Song Yang helped establish patient-derived organoids. Li-Ping Ge, Zong-Chao Gou and Xiao-En Xu revised the manuscript. Yi-Zhou Jiang conceived and oversaw the study. Zhi-Ming Shao and Yi-Zhou Jiang obtained funding. All authors read and approved the final manuscript.

Availability of data and materials

All data and materials can be provided upon request.

Competing Interests

The authors have declared that no competing interest exists.

References

1. Bray F, Ferlay J, Soerjomataram I, Siegel RL, Torre LA, Jemal A. Global cancer statistics 2018: GLOBOCAN estimates of incidence and mortality worldwide for 36 cancers in 185 countries. *CA Cancer J Clin.* 2018; 68: 394-424.
2. Cancer Genome Atlas N. Comprehensive molecular portraits of human breast tumours. *Nature.* 2012; 490: 61-70.
3. Carey LA, Dees EC, Sawyer L, Gatti L, Moore DT, Collichio F et al. The triple negative paradox: primary tumor chemosensitivity of breast cancer subtypes. *Clin Cancer Res.* 2007; 13: 2329-2334.
4. Foulkes WD, Smith IE, Reis-Filho JS. Triple-negative breast cancer. *N Engl J Med.* 2010; 363: 1938-1948.
5. Jiang YZ, Ma D, Suo C, Shi J, Xue M, Hu X et al. Genomic and Transcriptomic Landscape of Triple-Negative Breast Cancers: Subtypes and Treatment Strategies. *Cancer Cell.* 2019; 35: 428-440 e425.
6. Zhou L, Wang D, Sheng D, Xu J, Chen W, Qin Y et al. NOTCH4 maintains quiescent mesenchymal-like breast cancer stem cells via transcriptionally activating SLUG and GAS1 in triple-negative breast cancer. *Theranostics.* 2020; 10: 2405-2421.
7. Cheung A, Opzommer J, Ilieva KM, Gazinska P, Hoffmann RM, Mirza H et al. Anti-Folate Receptor Alpha-Directed Antibody Therapies Restrict the Growth of Triple-negative Breast Cancer. *Clin Cancer Res.* 2018; 24: 5098-5111.
8. Nirmala JG, Lopus M. Tryptone-stabilized gold nanoparticles induce unipolar clustering of supernumerary centrosomes and G1 arrest in triple-negative breast cancer cells. *Sci Rep.* 2019; 9: 19126.
9. Denkert C, Liedtke C, Tutt A, von Minckwitz G. Molecular alterations in triple-negative breast cancer—the road to new treatment strategies. *Lancet.* 2017; 389: 2430-2442.
10. Liedtke C, Mazouni C, Hess KR, Andre F, Tordai A, Mejia JA et al. Response to neoadjuvant therapy and long-term survival in patients with triple-negative breast cancer. *J Clin Oncol.* 2008; 26: 1275-1281.
11. Chang JC, Wooten EC, Tsimelzon A, Hilsenbeck SG, Gutierrez MC, Tham YL et al. Patterns of resistance and incomplete response to docetaxel by gene expression profiling in breast cancer patients. *J Clin Oncol.* 2005; 23: 1169-1177.
12. Ayers M, Symmans WF, Stec J, Damokosh AJ, Clark E, Hess K et al. Gene expression profiles predict complete pathologic response to neoadjuvant paclitaxel and fluorouracil, doxorubicin, and cyclophosphamide chemotherapy in breast cancer. *J Clin Oncol.* 2004; 22: 2284-2293.
13. Iwao-Koizumi K, Matoba R, Ueno N, Kim SJ, Ando A, Miyoshi Y et al. Prediction of docetaxel response in human breast cancer by gene expression profiling. *J Clin Oncol.* 2005; 23: 422-431.
14. Thuerigen O, Schneeweiss A, Toedt G, Warnat P, Hahn M, Kramer H et al. Gene expression signature predicting pathologic complete response with gemcitabine, epirubicin, and docetaxel in primary breast cancer. *J Clin Oncol.* 2006; 24: 1839-1845.
15. Balko JM, Cook RS, Vaught DB, Kuba MG, Miller TW, Bhola NE et al. Profiling of residual breast cancers after neoadjuvant chemotherapy identifies DUSP4 deficiency as a mechanism of drug resistance. *Nat Med.* 2012; 18: 1052-1059.
16. Balko JM, Giltman JM, Wang K, Schwarz LJ, Young CD, Cook RS et al. Molecular profiling of the residual disease of triple-negative breast cancers

- after neoadjuvant chemotherapy identifies actionable therapeutic targets. *Cancer Discov.* 2014; 4: 232-245.
17. Balko JM, Schwarz LJ, Luo N, Estrada MV, Giltneane JM, Davila-Gonzalez D et al. Triple-negative breast cancers with amplification of JAK2 at the 9p24 locus demonstrate JAK2-specific dependence. *Sci Transl Med.* 2016; 8: 334ra353.
 18. Kim C, Gao R, Sei E, Brandt R, Hartman J, Hatschek T et al. Chemoresistance Evolution in Triple-Negative Breast Cancer Delineated by Single-Cell Sequencing. *Cell.* 2018; 173: 879-893 e813.
 19. Boichuk S, Galebikova A, Sitenkov A, Khusnutdinov R, Dunaev P, Valeeva E et al. Establishment and characterization of a triple negative basal-like breast cancer cell line with multi-drug resistance. *Oncol Lett.* 2017; 14: 5039-5045.
 20. Rouzier R, Rajan R, Wagner P, Hess KR, Gold DL, Stec J et al. Microtubule-associated protein tau: a marker of paclitaxel sensitivity in breast cancer. *Proc Natl Acad Sci U S A.* 2005; 102: 8315-8320.
 21. Kavallaris M. Microtubules and resistance to tubulin-binding agents. *Nat Rev Cancer.* 2010; 10: 194-204.
 22. Prieto-Vila M, Takahashi RU, Usaba W, Kohama I, Ochiya T. Drug Resistance Driven by Cancer Stem Cells and Their Niche. *Int J Mol Sci.* 2017; 18.
 23. Phi LTH, Sari IN, Yang YG, Lee SH, Jun N, Kim KS et al. Cancer Stem Cells (CSCs) in Drug Resistance and their Therapeutic Implications in Cancer Treatment. *Stem Cells Int.* 2018; 2018: 5416923.
 24. Chi Y, Xue J, Huang S, Xiu B, Su Y, Wang W et al. CapG promotes resistance to paclitaxel in breast cancer through transactivation of PIK3R1/P50. *Theranostics.* 2019; 9: 6840-6855.
 25. Yin J, Lang T, Cun D, Zheng Z, Huang Y, Yin Q et al. pH-Sensitive Nano-Complexes Overcome Drug Resistance and Inhibit Metastasis of Breast Cancer by Silencing Akt Expression. *Theranostics.* 2017; 7: 4204-4216.
 26. Dobin A, Davis CA, Schlesinger F, Drenkow J, Zaleski C, Jha S et al. STAR: ultrafast universal RNA-seq aligner. *Bioinformatics.* 2013; 29: 15-21.
 27. Li B, Dewey CN. RSEM: accurate transcript quantification from RNA-Seq data with or without a reference genome. *BMC Bioinformatics.* 2011; 12: 323.
 28. Kanehisa M, Goto S. KEGG: kyoto encyclopedia of genes and genomes. *Nucleic Acids Res.* 2000; 28: 27-30.
 29. Subramanian A, Tamayo P, Mootha VK, Mukherjee S, Ebert BL, Gillette MA et al. Gene set enrichment analysis: a knowledge-based approach for interpreting genome-wide expression profiles. *Proc Natl Acad Sci U S A.* 2005; 102: 15545-15550.
 30. Liberzon A, Birger C, Thorvaldsdottir H, Ghandi M, Mesirov JP, Tamayo P. The Molecular Signatures Database (MSigDB) hallmark gene set collection. *Cell Syst.* 2015; 1: 417-425.
 31. Jiang YZ, Yu KD, Peng WT, Di GH, Wu J, Liu GY et al. Enriched variations in TEK14 and breast cancer resistance to paclitaxel. *Nat Commun.* 2014; 5: 3802.
 32. Swanton C, Marani M, Pardo O, Warne PH, Kelly G, Sahai E et al. Regulators of mitotic arrest and ceramide metabolism are determinants of sensitivity to paclitaxel and other chemotherapeutic drugs. *Cancer Cell.* 2007; 11: 498-512.
 33. Walsh AJ, Cook RS, Skala MC. Functional Optical Imaging of Primary Human Tumor Organoids: Development of a Personalized Drug Screen. *J Nucl Med.* 2017; 58: 1367-1372.
 34. Sachs N, de Ligt J, Kopper O, Gogola E, Bounova G, Weeber F et al. A Living Biobank of Breast Cancer Organoids Captures Disease Heterogeneity. *Cell.* 2018; 172: 373-386 e310.
 35. Van Lidth de Jeude JF, Vermeulen JL, Montenegro-Miranda PS, Van den Brink GR, Heijmans J. A protocol for lentiviral transduction and downstream analysis of intestinal organoids. *J Vis Exp.* 2015.
 36. Hari M, Loganzo F, Annable T, Tan X, Musto S, Morilla DB et al. Paclitaxel-resistant cells have a mutation in the paclitaxel-binding region of beta-tubulin (Asp26Glu) and less stable microtubules. *Mol Cancer Ther.* 2006; 5: 270-278.
 37. Gao J, Huo L, Sun X, Liu M, Li D, Dong JT et al. The tumor suppressor CYLD regulates microtubule dynamics and plays a role in cell migration. *J Biol Chem.* 2008; 283: 8802-8809.
 38. Matov A, Applegate K, Kumar P, Thoma C, Krek W, Danuser G et al. Analysis of microtubule dynamic instability using a plus-end growth marker. *Nat Methods.* 2010; 7: 761-768.
 39. Zhao S, Liu XY, Jin X, Ma D, Xiao Y, Shao ZM et al. Molecular portraits and trastuzumab responsiveness of estrogen receptor-positive, progesterone receptor-positive, and HER2-positive breast cancer. *Theranostics.* 2019; 9: 4935-4945.
 40. Al-Dhifan A, Alhoshani A, Korashy HM. Aryl hydrocarbon receptor/cytochrome P450 1A1 pathway mediates breast cancer stem cells expansion through PTEN inhibition and beta-Catenin and Akt activation. *Mol Cancer.* 2017; 16: 14.
 41. Ahmed AA, Lu Z, Jennings NB, Etemadmoghadam D, Capalbo L, Jacamo RO et al. SIK2 is a centrosome kinase required for bipolar mitotic spindle formation that provides a potential target for therapy in ovarian cancer. *Cancer Cell.* 2010; 18: 109-121.
 42. Ianevski A, Giri AK, Aittokallio T. SynergyFinder 2.0: visual analytics of multi-drug combination synergies. *Nucleic Acids Res.* 2020; 48: W488-W493.
 43. Nagy A, Lanczky A, Menyhart O, Gyorffy B. Validation of miRNA prognostic power in hepatocellular carcinoma using expression data of independent datasets. *Sci Rep.* 2018; 8: 9227.
 44. Karaayvaz M, Cristea S, Gillespie SM, Patel AP, Mylvaganam R, Luo CC et al. Unravelling subclonal heterogeneity and aggressive disease states in TNBC through single-cell RNA-seq. *Nat Commun.* 2018; 9: 3588.
 45. Binder JX, Pletscher-Frankild S, Tsafou K, Stolte C, O'Donoghue SI, Schneider R et al. COMPARTMENTS: unification and visualization of protein subcellular localization evidence. *Database (Oxford).* 2014; 2014: bau012.
 46. Rouillard AD, Gundersen GW, Fernandez NF, Wang Z, Monteiro CD, McDermott MG et al. The harmonizome: a collection of processed datasets gathered to serve and mine knowledge about genes and proteins. *Database (Oxford).* 2016; 2016.
 47. Horwitz SB. Taxol (paclitaxel): mechanisms of action. *Ann Oncol.* 1994; 5 Suppl 6: S3-6.
 48. Palazzo A, Ackerman B, Gundersen GG. Cell biology: Tubulin acetylation and cell motility. *Nature.* 2003; 421: 230.
 49. Navin NE. Tumor evolution in response to chemotherapy: phenotype versus genotype. *Cell Rep.* 2014; 6: 417-419.
 50. Morris PG, Fournier MN. Microtubule active agents: beyond the taxane frontier. *Clin Cancer Res.* 2008; 14: 7167-7172.
 51. Galjart N, Perez F. A plus-end raft to control microtubule dynamics and function. *Curr Opin Cell Biol.* 2003; 15: 48-53.
 52. Balachandran R, Welsh MJ, Day BW. Altered levels and regulation of stathmin in paclitaxel-resistant ovarian cancer cells. *Oncogene.* 2003; 22: 8924-8930.
 53. Fukuda M. Rab27 effectors, pleiotropic regulators in secretory pathways. *Traffic.* 2013; 14: 949-963.
 54. Fukuda M. Slp4-a/granuphilin-a inhibits dense-core vesicle exocytosis through interaction with the GDP-bound form of Rab27A in PC12 cells. *J Biol Chem.* 2003; 278: 15390-15396.
 55. Tsuboi T, Fukuda M. The Slp4-a linker domain controls exocytosis through interaction with Munc18-1/syntaxin-1a complex. *Mol Biol Cell.* 2006; 17: 2101-2112.
 56. Galvez-Santesteban M, Rodriguez-Fraticelli AE, Bryant DM, Vergarajaregui S, Yasuda T, Banon-Rodriguez I et al. Synaptotagmin-like proteins control the formation of a single apical membrane domain in epithelial cells. *Nat Cell Biol.* 2012; 14: 838-849.
 57. Bierings R, Hellen N, Kiskin N, Knipe L, Fonseca AV, Patel B et al. The interplay between the Rab27A effectors Slp4-a and MyRIP controls hormone-evoked Weibel-Palade body exocytosis. *Blood.* 2012; 120: 2757-2767.
 58. Adam F, Kauskot A, Kurowska M, Goudin N, Munoz I, Bordet JC et al. Kinesin-1 Is a New Actor Involved in Platelet Secretion and Thrombus Stability. *Arterioscler Thromb Vasc Biol.* 2018; 38: 1037-1051.